OBSERVATIONS OF VERTICAL EDDY DIFFUSIVITIES IN A SHALLOW TROPICAL RESERVOIR

PEIPEI YANG[1], ZIKUN XING[1], DEREK A. FONG[2], STEPHEN G. MONISMITH[2]
KOK MENG TAN[3] AND EDMOND Y.M. LO[1]

Abstract
Tropical lakes are of key importance as fresh water supply sources in tropical regions. One of the biggest threats to tropical lakes is nuisance algal blooms which at times can be harmful to human health. Research shows that thermal and flow dynamics, through their effects on the light and nutrient accessibility to phytoplankton, have a strong bearing on the growth of phytoplankton. We report herein results combining long-term and the short-term observations of vertical diffusivities which impact the evolution of the surface mixed layer and the vertical transport of nutrients for a shallow tropical reservoir, Kranji Reservoir in Singapore.

The one-dimensional heat flux method (Jassby and Powell 1975; Henderson-Sellers 1985) is applied to obtain estimates of the vertical mixing in Kranji Reservoir using water temperature and meteorological data collected during a two month field experiment conducted in 2007. To fit the assumptions of the method and particularly the heating duration, a time period of 11:00-15:00 is selected for heat flux method when the water body is strongly stratified. The vertical eddy diffusivity, K_z varies with depth and spans two orders of magnitude, from 10^{-5} to 10^{-3} m^2/s. In addition, short-term observations from two 24hr turbulence microstructure measurements conducted in 2011 are considered. The heat flux method derived diffusivities are compared directly against those derived from the microstructure measurements with reasonable agreement with the latter when the system fits a one-dimensional assumption. The microstructure measurements further provides K_z observed values over the entire day and this is discussed in the context of the thermal forcing regimes in Kranji reservoir.

Keywords: Shallow tropical lakes, vertical eddy diffusivities, heat flux method, SCAMP

[1] School of Civil and Environmental Engineering,
Nanyang Technological University, 50 Nanyang Ave, Singapore 639798,
e-mail: c090086@ntu.edu.sg, zkxing@ntu.edu.sg, cymlo@ntu.edu.sg
[2]Dept. of Civil and Environmental Engineering, Stanford University,
Stanford, California, US, 94305-4020,
e-mail: dfong@stanford.edu, monismith@stanford.edu
[3] PUB, Singapore's national water agency, 40 Scotts Road #07-01 Environment Building Singapore 228231
e-mail: tan_kok_meng@pub.gov.sg

1. Introduction

Tropical lakes are of key importance as fresh water supply sources in tropical regions. However, compared to numerous studies done on their temperate counterparts, reported work on tropical lakes is limited (Lewis 1996) and even less is known about shallow tropical lakes. Different from the temperate lakes, tropical lakes experience a low-amplitude annual temperature cycle and thus exhibit a lower stability of the water column than temperate lakes. In deep tropical lakes, a diel cycle of stratification is observed near the water surface, superimposed upon a persistent deeper seasonal stratification (MacIntyre and Melack 1982); while in shallow tropical lakes, the stratification can be easily destroyed by a small amount of heat loss during night time cooling or storm events. Complete mixing occurs multiple times per year and in some shallow tropical lakes such as Lake George (Ganf 1974), even on a daily basis.

The study site considered here is Kranji reservoir (1˚25'N, 103˚43'E) in Singapore, which has an average depth of about 5 m. Similar to other shallow tropical lakes, it stratifies and destratifies diurnally (Xing et al. 2014). The NTU-PUB Kranji Project (Lo 2008) showed that Kranji was eutrophic, experiencing intermittent Microcystis blooms throughout the study period (2005 to 2007). Xing et al. (2014) showed that Kranji reservoir could respond in three different thermal forcing regimes: (a) solar driven, (b) windy and (c) cold inflow with the solar driven being the most commonly observed regime. Similar variations can thus be expected for the vertical mixing and an understanding of this is important since the vertical mixing determines how much the light and nutrient phytoplankton can gain for its growth (MacIntyre 1993; Huisman et al. 1999; Wong et al. 2007) and is central to the interaction between the physical processes and algal dynamics.

The vertical eddy diffusivity is often used to characterize the vertical mixing by analogy to molecular diffusion (Pope 2000). A large body of work has been done to develop vertical diffusivity models based on field observation and numerical simulation. For the latter DNS, RANS and LES have been used to derive eddy viscosity values (e.g. Durski et al. 2004; Shih et al. 2005; Burchard et al. 2008). In this paper, we focus on field observations from which vertical diffusivity was derived from empirical models.

Sverdrup et al. (1942) proposed an empirical one-dimensional model for a depth-averaged vertical eddy diffusivity induced by wind mixing in the surface layer of coastal seas. The heat flux method is another common model for empirical derivation of the vertical eddy diffusivity based on the one-dimensional vertical heat transport equation (Jassby and Powell 1975; Henderson-Sellers 1985; Yeates and Imberger 2003). Osborn and Cox (1972) derived vertical eddy diffusivities directly from the temperature variance χ_T : $K_z = \frac{1}{2}\chi_T \Big/ \left(\frac{\partial \overline{T}}{\partial z}\right)^2$, by assuming the turbulence-generated temperature fluctuations in a spatial mean temperature gradient $\frac{\partial \overline{T}}{\partial z}$ is equal to its dissipation due to molecular diffusion. Osborn (1980) found that the vertical eddy diffusivity depends on the mixing efficiency (Γ) and the dissipation of turbulent kinetic energy (ε), and inversely proportional to the stratification (*N*): $K_z = \Gamma \varepsilon / N^2$, and suggested 0.2 as a critical value for the mixing efficiency. Alternatively, Ivey and Imberger (1991) parameterized the mixing efficiency with the turbulent Froude number and turbulent Reynolds number, and Shih et al. (2005) estimated the behaviour of mixing efficiency relative to an turbulent intensity parameter $\varepsilon/(\nu N^2)$ and found best fits of K_z in three distinct regimes of $\varepsilon/(\nu N^2)$.

Due to easy access to temperature records, the heat flux method is suitable for long term monitoring of the vertical diffusivity. This method has been previously applied to temperate lakes (Jassby and Powell 1975; Benoit and Hemond 1996) and deep tropical lakes (Lewis 1982). The estimation of the K_z was made based on the temperature profiles averaged over several days, for example, over 2.5 days in Jassby and Powell 1975

and over 10-15 days in Benoit and Hemond 1996. Few attempts, however, have been made at applying the method to shallow tropical systems such as the Kranji reservoir, where complete mixing occurs almost on daily basis. Here we report results combining long-term observation of vertical eddy diffusivities using the heat flux method based on a two-month temperature measurement in 2007 from 13 Apr (year day 103) to 10 Jun (year day 161) and short-term observations based on two 24hr periods of turbulence microstructure measurements on Sept 29/30 and Oct 5/6 2011. By combining these observations we examine the accuracy of the heat flux method relative to the microstructure measurements. We also provide observations of the vertical eddy diffusivity for the two 24hr periods, which while limited to 2 days, were in two separate distinct thermal forcing regimes as reported in Xing et al. (2014).

2. Material and Methods

Study site

Kranji Reservoir (see Figure 1) is located in the northwest corner of Singapore. It has a catchment area of about 5600 ha, a reservoir surface area of about $3x10^6$ m^2 and an average depth of about 5m. The reservoir is mainly supplied by the runoff brought in by four tributaries, namely Sg. Kangkar, Sg. Tengah, Sg. Pengsiang, and Sg. Pangsua, and the direct rainfall on the reservoir. Like many other shallow tropical lakes, Kranji reservoir is a polymictic lake with diurnal cycles of thermal stratification and destratification.

Figure 1

Data Collection

The work presented here draws upon physical field data collected at three mooring stations M4, M5 and M6 (Figure 1) during a field experiment in 2007 from Apr 13 (year day 103) to Jun 10 (year day 161) as reported in Xing et al. (2012). M4, about 6 m deep, is at the junction of three tributaries, Sg. Kangkar, Sg. Tengah, and Sg. Pengsiang. M5 located near the tributary Sg. Pangsua is 8.4 m deep and M6 has a depth of 13 m which is very close to the deepest depth location in Kranji Reservoir. The temperature at M4 and M5 was monitored with thermistor chains comprised of 5 and 7 Seabird SBE-39 thermistors respectively, at 1 m vertical spacing. At M6 the temperature was monitored with 9 thermistors with the vertical spacing of 1 m between the depth 1 m to 7 m and 2 m spacing between the depths 7 m to 11 m. The thermistors have an accuracy of 0.002 degrees Celsius and the first thermistor was located at 1m below the water surface at all the stations.

A meteorological station set up near M5 provided air temperature, relative humidity, wind speed and direction, shortwave radiation, and rainfall at 15 minutes intervals. There was a break in the meteorological data record from May 6 (year day 126) to May 15 (year day 135) 2007, due to equipment malfunction.

An additional field exercise was further conducted from Sept 19 to Oct 10 2011. A Precision Measurement Engineering Self-Contained Autonomous MicroProfiler (SCAMP) was used to measure the temperature microstructure near M5 (Figure 1) for two 24-hour periods (over Sept 29/30 and Oct 5/6), making 8 SCAMP casts per hour. SCAMP sampled at a frequency of 100 Hz while rising up to the surface at 10 cm/s, which resulted in a spatial resolution of about 1 mm. Flow velocity data was also collected with a bottom-mounted 1200 KHz Teledyne RDI Acoustic Doppler Current Profiler (ADCP). The bin size was set as 0.5m. The ensemble interval was 12s and each ensemble contained 80 sub-pings with an uncertainty of ±0.78 cm/s.

3. Data Analysis

Heat flux method

Assuming negligible heat transfer through inflows and outflows as well as through the bottom, a one-dimensional eddy diffusion model can be used to predict the water temperature as a function of vertical

mixing and depth-dependent solar heating. The assumption of negligible bottom heat transfer is valid because of the small heat flux to the sediment (see Figure 3 and the discussion below) as compared to the incoming solar irradiance of 100-1000 W/m^2. During the solar forcing regime in the reservoir (regime classifications reported in Xing et al. 2014), the thermal structure is primarily forced by shortwave radiation such that the thermal stratification is largely one-dimensional with the temperature difference between the surface and bottom water being strongly correlated with the daily solar radiation. By simplification via removing the area dependence, i.e., constant lake area (Henderson-Sellers 1985), the vertical eddy diffusivity is expressed as:

$$K_z(z) = \frac{1}{\left(-\partial T / \partial z\big|_z\right)}\left(\frac{\partial}{\partial t}\int_z^{z_m} T(\zeta)\,d\zeta - R(z)\big|_z / c_h\rho\right) \qquad \text{[Eq.1]}$$

where K_z denotes the vertical eddy diffusivity, T is the temperature, z is the vertical depth (positive upwards), R(z) is the surface flux, c_h is the specific heat capacity of water and ρ is the water density. About 9% of the incident short-wave irradiance was reflected from the water surface at Kranji, i.e., the albedo was about 0.09 measured via the Kipp & Zonen NR-LITE-L5 4-channel radiometer during the 2007 field work. A large portion of the short-wave irradiance is also absorbed in the uppermost 1-2 mm of the water body (Henderson-Sellers 1986) and this is assumed to be about 55% (Moon 1940; Tsubo and Walker 2005; Imerito 2007). The remainder also known as photosynthetically active radiation (PAR), penetrates into the water column and is the heat source R(z) for [Eq.1] above:

$$R(z) = (1-0.09)\,R_{short-wave}\cdot(1-0.55)\cdot\exp(-k_s z) \qquad \text{[Eq.2]}$$

where $R_{short\text{-}wave}$ is the incident short wave solar radiation; z is the water depth (positive downwards). The light intensity extinction coefficient, k_s was estimated via linear regression of light intensity (measured by a light meter, LiCor LI 1400) to the Lambert-Beer equation yielding a k_s of about 2 m^{-1} for the 2007 field exercise and 2.3 m^{-1} for 2011. k_s depended on the surface chlorophyll concentration which ranged over 50-70 $\mu g/l$ during the heating periods of the field experiments.

In implementation below, a block average of 2 hours was performed on the measured temperature data. The depth variations in temperature and temporal gradient with time were calculated using central-differences in space and forward in time. The time step was 2 hours and the vertical bin spacing was 0.5m. Linear interpolation of temperature between thermistor locations was used to obtain temperature gradients at 0.5 m spacing.

Heat loss to the sediment

The numerical model by Benoit and Hemond (1996) is used to calculate the heat flux between the water column and the sediment and thereby assess its effect. The governing equation for the sediment heating or cooling is

$$\frac{\partial T(z_{sed},t)}{\partial t} = \frac{K}{\rho_{sed} C_p} \times \frac{\partial^2 T(z_{sed},t)}{\partial {z_{sed}}^2} \qquad \text{[Eq.3]}$$

where z_{sed} denotes the depth into the sediment (positive downwards), ρ the sediment density (assumed 2000 kg/m^3), K the sediment thermal conductivity and C_p is the sediment heat capacity. The initial condition was set as the sediment temperature being equal to the average overlying water temperature $\overline{T_w} : T(z,0) = \overline{T_w}$. For

t>0, the temperature at the sediment-water interface (z_{sed} =0) was set equal to the overlaying water temperature $T(0,t)=T_w$ and the sediment was assumed to be semi-infinite with $T(\infty,t)=\overline{T_w}$.

Estimates of uncertainty

For obtaining uncertainty estimates of derived K_z, Eq. 1 can be re-written into as a function of variables a, b and c:

$$K_z(a,b,c)=\frac{1}{a}(b-c) \qquad \text{[Eq.4]}$$

where the uncertainties of a, b and c are given as $\sigma_a^2=\sigma_T^2\left(\frac{1}{\Delta z}\right)^2$; $\sigma_b^2=\sigma_T^2\sum_z^{z_m}\left(\frac{\Delta z}{\Delta t}\right)^2$; $\sigma_c^2=\sigma_{R_z}^2\,(1/c_h\rho)^2$.

Here $\sigma_T=0.002°C$ was set based on the maximum thermister instrument uncertainty and $\sigma_{Rz}=0.28W/m^2$ due to the accuracy of the radiometer Kipp & Zonen NR-LITE-L5 being about 3% of the readings and 96 samples were used in averaging (Xing et al. 2012). Assuming errors from the numerical scheme itself were negligible due to the 2-hour block averaging, the uncertainty in K_z arose from instrument precision which then followed the standard propagation error equation (Bevington 1994):

$$\sigma_{K_z}^2=\sigma_a^2\left(\frac{\partial K_z}{\partial a}\right)^2+\sigma_b^2\left(\frac{\partial K_z}{\partial b}\right)^2+\sigma_c^2\left(\frac{\partial K_z}{\partial c}\right)^2 \qquad \text{[Eq.5]}$$

Processing of SCAMP data

K_z can be derived from SCAMP profiles via the expression given in Osborn and Cox's (1972)

$$K_z=\frac{\frac{1}{2}\chi_T}{\left(\frac{\partial\overline{T}}{\partial z}\right)^2} \qquad \text{[Eq.6]}$$

where χ_T denotes the temperature variance, $\overline{T}$ the mean temperature and z depth below the surface (positive upwards). As χ_T in Eq. 6 is directly measured by SCAMP, K_z from χ_T as a direct measurement of vertical eddy diffusivities can be used to evaluate the accuracy of the heat flux method.

Following MacIntyre et al. (1999), the SCAMP temperature data was also used to calculate the dissipation rate of turbulent kinetic energy ε and the turbulent intensity parameter $\varepsilon/(\nu N^2)$ with *N* being the buoyancy frequency as deduced from the temperature microstructure. The turbulence activity was further classified into one of the three regimes based on the turbulence intensity parameter shown in Table 1 as reproduced from Shih et al. (2005), which aided in the interpretation of the K_z values.

Table 1

The gradient Richardson number is defined as

$$Ri_g=N^2/S^2 \qquad \text{[Eq.7]}$$

where N is the buoyancy frequency and S is the velocity shear rate in vertical direction, $S^2 = \left(\partial U / \partial z\right)^2 + \left(\partial V / \partial z\right)^2$ where the horizontal velocities U,V were obtained by filtering the ADCP measured velocities with a low-pass Butterworth filter with a normalized cut-off frequency corresponding to 5 minutes. Due to the high vertical resolution of SCAMP, spline smoothing was used to obtain a better fit than linear interpolation in the estimation of the velocity shear rate.

4. Results and Discussion

In applying the heat flux method, we isolated the analysis to a four hour window of 11:00-15:00 during the solar dominated regime i.e. when the strongest heating during the day occurred (see the short-wave radiation in Figure 2C) and stratification dynamics were most likely one-dimensional. If other time periods were included, negative non-physical K_z values (Figure 2B) were possible, due to the decreasing temperature with time (Figure 2A for e.g. 5:00-9:00 on day 110 of 2007).

The calculated heat exchange to the sediments over the 2007 field exercise period was of order 1 W/m^2 to 10 W/m^2 (Figure 3) for M5 with similar results for M4 and M6. This was very small compared to the solar irradiance of 100-1000 W/m^2 (see Figure 2C), and thus subsequently neglected.

Figure 2

Figure 3

Representative temperature profiles along the main channel at M4, M5 and M6 during the heating stage (time of 11:00-15:00) on day 110 in 2007 when the water body was stratified are shown in the left panel of Figure 4. The temperature profiles were characterized by small temperature differences of about 0.5~2^{o}C between the surface thermistor (1 m below the surface) and the bottom thermistor. A diurnal thermocline occurred at about 1 m below the surface. Correspondingly, small vertical eddy diffusivities were observed in the same part of the water column (Figure 4, right panel). The values then increased with a maximum of K_z just beneath the thermocline. A homogenous mixing layer was observed over the depth 4 m to 6 m at M5 and over the depth 4 m to 7 m at M6 with small variation of K_z values. Below this layer, the vertical eddy diffusivities began to decrease with the depth towards the bottom. The large error bars in the lower water column at M6 were caused by the combined effects of the small temperature spatial and temporal gradients as a result of M6 being the deepest with depth of 13 m. The K_z values from the heat flux method in Kranji reservoir ranged from 10^{-5} to 10^{-3} m^2/s, these values similar to those obtained from other studies (e.g. Imboden et al. 1983; MacIntyre 1993).

The median eddy diffusivities from the depth profiles of diffusivities over the 43 solar regime days of the field deployment period (Xing et al. 2014) are presented in Figure 5 with the bars covering the ranges from the 1st quartile to the 3rd quartile of K_z values. The vertical pattern of K_z in Figure 5 is similar to in Figure 4. A horizontal variation was observed for the three measurement sites with the maximum values at M6. The K_z values at M4 and M5 ranged from 10^{-5} to 10^{-4} m^2/s, while the median K_z values at M6 were an order of magnitude larger from 10^{-4} to 10^{-3} m^2/s. Temperature changes are smaller during daytime heating at the deeper locations than in shallower ones in the same reservoir (Monismith et al. 1990). As a result, the stronger vertical stratification was built up at M5 (8.4 m) and at M4 (6 m) than at M6 (13 m), as also shown by the temperature profiles of day 110 in Figure 4. Correspondingly smaller K_z values were obtained at M4 and M5 as shown in Figure 5.

We also applied the heat flux method for other hydro-meteorological conditions of windy and cold inflow days though the 1D heating assumption was not strictly fulfilled and the number of observed days was limited (4 for windy and 3 for cold inflow). The median values of K_z at M6 during the different regimes are shown in

Figure 6. During the solar days, the small K_z values in the upper water column indicated strong stratification. In contrast, during the windy days, the large K_z in the upper water column reflected strong wind mixing in the surface layer. The K_z trend in the lower water column remained the same during both regimes. The vertical eddy diffusivity in the cold inflow regime denoted by the dotted line had generally small K_z values reflecting the enhancement of stratification by the cold underflows. These K_z results were consistent with the thermal forcing regimes observed by Xing et al. 2014. The heat flux method thus could qualitatively characterize the variation of vertical eddy diffusivities in responses to different meteorological conditions even though system was not strictly one-dimensional in the non-solar days. Further examination was next done by using observations made via microstructure measurements.

Figure 4

Figure 5

Figure 6

Direct measurements of K_z were derived via Eq. 6 based on the temperature variance χ_T from SCAMP temperature microstructure measurements carried out near M5 over two 24hr periods of 11:00 Sept 29-11:00 Sept 30 and 12:00 Oct 5-12:00 Oct 6, 2011. The hydro-meteorological conditions are shown in Figure 7. The hydro-meteorological conditions were very different on the two days. On Sept 29/30, two rainfall events occurred on mornings of the 29th and 30th (Figure 7F) during which the wind speeds, at times, exceeded 5 m/s (Figure 7C). In contrast, no precipitation was measured on Oct 5/6 with high wind speeds> 5m/s only observed during 12:00-15:00 in Figure 7D. Both Figure 7A and 7B show the shortwave solar radiation occurred over 7:00 to 19:00. Here we define the heating period as 11:00-19:00 for Sept 29/30 and 12:00-19:00 for Oct 5/6 and the non-heating period as 19:00-7:00 for both 24hr SCAMP measurements to facilitate the discussion. The duration of the two heating periods were slightly different because the 24hr SCAMP profiling started at 11:00 on Sept 29 while it did not begin until 12:00 on Oct 5/6. The short-wave radiation had an average of 460 W/m^2 during 11:00-19:00 Sept 29 and an average of 305 W/m^2 during 12:00-19:00 Oct 5. Although the solar radiation of Sept 29 was stronger, the water column on Oct 5 was more stratified than on Sept 29. The maximum temperature difference during Sept 29/30 was about 1^{o}C and most of the ΔT values were below 0.5 ^{o}C (Figure 8C). In contrast, the maximum ΔT during Oct 5/6 was about 2.5 ^{o}C (Figure 8D) and ΔT was larger than 1 ^{o}C except for the short early morning 5:00-9:00 period on Oct 6. This was due to a large inflow plunging into the reservoir on Oct 4 (Figure 7G) which kept the temperature of the deeper water below 29 ^{o}C over Oct 5/6, thus enhancing the stratification. The very different thermal structures were then observed (see Figures 8A and 8B) during the two 24hr SCAMP periods, separated by only five days. Following Xing et al's (2014) thermal regime classification Sept 29/30 was a solar driven day and Oct 5/6 was a cold inflow day,.

The SCAMP microstructure profiles also allowed us to compare the strength of vertical mixing in the context of the two different thermal forcing regimes, i.e., solar and cold inflow regimes, via the vertical eddy diffusivities derived from χ_T. The vertical diffusivities K_z together with the gradient Richardson number (Ri_g) and the turbulent intensity parameter $\varepsilon/(\nu N^2)$ are plotted in Figure 9. Different vertical eddy diffusivities structures were observed during the two regimes. The vertical structure during Oct 5/6 (cold inflow day) was clearly three-layered. The cold inflow kept the lower water column cooled from the bottom i.e., the isotherms did not shift downwards during the heating period of Oct 5 and displaced upwards during the non-heating period of Oct 5/6. As a result, the thermocline during Oct 5/6 remained in the depth range of 2 to 5 m. The thermocline as reflected by a band of small K_z, large Ri_g and small $\varepsilon/(\nu N^2)$ (see Figures 9B, 9D and 9F) divided the vertical water column into three layers:

(i) thin surface layer (0-2m depth) mixed by the wind with velocity shear overcoming buoyancy (70% of $Ri_g<0.25$), energetic turbulence (65% of $\varepsilon/(\nu N^2)$ >100) and a depth-median of K_z of $2.1x10^{-5}$ m^2/s over the surface layer.
(ii) calm thermocline (over 2-5m depth) with buoyancy dominating (69% of $Ri_g>1$, 68% of $\varepsilon/(\nu N^2)<100$) and a depth-median K_z of $7.4x10^{-7}$ m^2/s over the thermocline during the heating period and $4.3x10^{-7}$ m^2/s during the non-heating period, and
(iii) lower water column below 5m as stirred by intermittent strong turbulence patches from the cold inflow with 31% of $Ri_g<0.25$, 70% of $Ri_g<1$, 64% of $\varepsilon/(\nu N^2)$ >100 and depth-median K_z of $1.6x10^{-5}$ m^2/s during the heating period and $8.5x10^{-5}$ m^2/s during the non-heating period.

The heating-period vertical structure during Sept 29/30 (solar driven day) was also three-layered but not as distinct as during Oct 5/6. The upper water column was stratified during the heating period of Sept 29: the surface layer thickness was of ~1m with the depth-median K_z of $2.3x10^{-4}m^2/s$ over this thin layer and the thermocline with a depth-median K_z of $2.8x10^{-5}$ m^2/s in the water depth of 1.5-2.5 m. Small values of $\varepsilon/(\nu N^2)$ and $Ri_g>0.25$ were also observed at the thermocline but the pattern was not as obvious as shown by K_z. Large $\varepsilon/(\nu N^2)$ and large K_z with a depth-median of $2.8x10^{-4}$ m^2/s were observed below the thermocline, which indicated the occurrence of strong turbulence in the lower water column. During the non-heating period of Sept 29/30, the vertical structure of water column was determined by differential cooling. The Kranji map in Figure 1 shows deeper water near the dam of up to 16 m deep and shallower water near the junction of about 5 m deep. The velocity along the channel during Sept 29/30 2011 is shown in Figure 8E with positive velocity towards the dam and negative towards the junction. The surface water was heated up during 20:00-3:00 of Sept 29/30 in Figure 8A with the surface current towards the junction as shown in Figure 8E while the strong submerged flow in the lower water column was towards the dam, which was evidence of differential cooling. The surface warm current from the dam heated the surface water near M5 and the cold flow from the junction cooled the water near the bottom down. Different from the heating period, there was no strong thermocline region during this period. Thus the water column was considered as two-layered. The depth-median K_z was $2.0x10^{-4}$ m^2/s within the surface weak negative current and was $3.1x10^{-4}$ m^2/s within the bottom positive underflow as shown in Figure 8E. The depth-median K_z value over the whole water column as listed in Table 2 reflected a diurnal variation of vertical mixing responding to the diurnal cycle of the thermal stratification: the stronger vertical mixing during the non-heating period than the heating period was also in agreement with the smaller temperature difference (<0.5 ^oC) from 19:00 to 7:00 and the larger temperature difference of about 1^oC from 11:00 to 19:00 as shown in Figure 8C.

We summarized in Table 2 the depth-median K_z values observed in the surface layer, the thermocline and the lower water column over the two SCAMP days reflecting the two different forcing regimes. The K_z values during the solar-driven day (Sept 29/30) were much higher than those during the cold inflow day (Oct 5/6). The depth-median K_z over the whole water column during the heating period of Sept 29 (11:00-19:00) was about $1.8x10^{-4}$ m^2/s, nearly two orders of magnitude larger than that of $3.6x10^{-6}$ m^2/s during the same period of Oct 5. The vertical mixing was significantly suppressed in the cold inflow regime, which was qualitatively consistent with the variation of K_z calculated by the heat flux method in the forcing regimes as shown in Figure 6. It is noted from Table 2 that the mixing strength in the lower water column as evaluated by the magnitude of K_z, was comparable to that in the surface mixed layer and much stronger than in the thermocline. There were inflows on both SCAMP days as shown in Figure 7E: the small inflow due to the early morning rain of Sept 29 and the inflow throughout the entire 24hr measurement period of Oct 5/6, which might be responsible for the strong mixing in the lower water column. In addition, the mixing during the non-heating period in the lower water column during Sept 29/30 was attributed to the underflow generated by differential cooling.

Table 2

Figure 7

Figure 8

Figure 9

The SCAMP temperature measurements carried out near M5 on Sept 29 2011 are shown in Figure 10 along with the corresponding K_z values derived from the temperature variance χ_T . The temperature profiles averaged over 2 hour periods over 11:00-15:00 are shown in Figure 10A, while the χ_T -derived K_z values over 11:00-15:00 are shown by the boxplot with a depth bin size of 0.5 m in Figure 10B. There was a sharp decrease of temperature with depth from the water surface which was not resolved in the earlier 2007 field experiment due to the latter having the first thermistor being located at 1 m below and further from the water surface. The temperature changed less with depth between 2 m to 6 m and then decreased with depth again. The large K_z values were observed near the surface and the bottom. The larger surface values were likely caused by intermittent surface winds which were not resolved in the 2007 field experiment. The large bottom values could be associated with the small inflow before 11:00 Sept 29 in Figure 7E. The small K_z seen in the depth between 1.5 to 2.5 m likely reflected the effects of vertical decay of wind stirring, and the increased importance of buoyancy within the thermocline. Similar to the earlier 2007 K_z values at M6 and M5 (Figures 4 and 5), there existed a homogenous mixing layer and the medians of K_z were about the same over the depth 3.5 to 6 m. The depth-median K_z over the whole water column derived from SCAMP for the heating period of Sept 29/30 2011 was of 1.8×10^{-4} m^2/s in the same order of magnitude as the depth-median K_z of 5.5×10^{-4} m^2/s calculated by the heat flux method over the 43 solar days (Figure 6) using the 2007 temperature data.

Finally, we evaluated the heat flux method by comparing K_z calculated from the SCAMP measured temperature profiles re-binned into 0.5 m spacing and using the heat flux method with those χ_T -deduced K_z. This comparison used the SCAMP data collected during Sept 29/30 2011 when the solar radiation was the dominant forcing and the system could be considered as one-dimensional. The $K_{z\ \text{heat flux method}}$ values are superimposed on the boxplot in Figure 10B. The solid line with circles denotes $K_{z\ \text{heat flux method}}$ during 11:00-13:00 and the dashed line with squares during 13:00-15:00. The results were in reasonable agreement. The vertical profile of $K_{z\ \text{heat flux method}}$ was similar to those derived from χ_T from the surface to a depth of 7m. We also observed suppressed mixing over the depth 1 to 2.5m with small K_z values and a homogenous mixing layer from 3.5 to 6m deep from the heat flux calculated K_z profile. However different trends were seen in the deeper part of the water column (7m to bottom) as the stirring effect by the inflow was not modelled by the heat flux method. Overall, the heat flux calculated values were generally within an order of magnitude compared to the median values of the 0.5-m bins (the middle line of the box) from the SCAMP measured χ_T . The differences were attributed to the inherent resolution of the heat flux method and that the instantaneous eddy viscosity values were highly variable as seen from the range of the boxplot SCAMP K_z values of Figure 10B. The corresponding comparison using the Oct 5/6 2011 SCAMP data, as expected, was not good (not shown) as the reservoir was in different thermal regime and the heat brought in by the inflow could not be neglected, i.e., the system was not one-dimensional.

Figure 10

5 Summary and Conclusions

Vertical diffusivity K_z values were obtained for Kranji reservoir using (i) the heat flux method and measured temperature profiles as input, and (ii) SCAMP measured microstructure profiles. It has been demonstrated that the thermal system of a tropical shallow reservoir is delicate and its response is not strictly one-dimensional. Because of the nature of the thermal system, the heat flux method only yielded meaningful results during the daily heating hours. This is in sharp contrast to temperate lakes where the heat flux method can typically be applied on the time scale of days e.g., 2.5 days for Castle Lake (Jassby and Powell 1975) and

10-15 days for Bickford Reservoir (Benoit and Hemond 1996). The restricted application of the heat flux method was further elucidated by the SCAMP microstructure measurements which showed that in spite of the delicate dynamic balance with small temperature gradients and mild temperature increases with time, the heat flux method does provide reasonable estimates of vertical diffusivity when the reservoir fits the one-dimensional assumption under solar radiation driven conditions. The SCAMP measurements, though limited to two 24 hr periods, furthermore revealed that the reservoir exhibited very different vertical structures and K_z values on two days which were only 5 days apart, corresponding to different thermal regimes of a solar heating day and a cold inflow day. Both the heat flux method and the SCAMP gave the depth-averaged K_z of the order of magnitude of 10^{-5} to 10^{-3} m^2/s on the solar heating days while on the day with cold inflow the depth-averaged K_z from SCAMP was on the order of magnitude of 10^{-5} m^2/s. These very different measured diffusivities, due to the different external forcing within the order of a few days, highlighted the strong variability inherent in shallow tropical lakes.

Acknowledgements

This work is supported by the Singapore Stanford Partnership Program and Singapore's National Research Foundation (NRF) under its Environmental and Water Technologies (EWT) PhD Scholarship Program. We also thank PUB, Singapore's national water agency for access to the field site and field support.

Reference

Benoit, G. and H. F. Hemond (1996). "Vertical eddy diffusion calculated by the flux gradient method: significance of sediment-water heat exchange." Limnology and Oceanography **41**(1): 12.

Bevington, P. R. (1994). Data reduction and error analysis for the physical sciences McGraw-Hill.

Burchard, H., P. D. Craig, J. R. Gemmrich, H. van Haren, P.-P. Mathieu, H. E. M. Meier, W. A. M. N. Smith, H. Prandke, T. P. Rippeth, E. D. Skyllingstad, W. D. Smyth, D. J. S. Welsh and H. W. Wijesekera (2008). "Observational and numerical modeling methods for quantifying coastal ocean turbulence and mixing." Progress in Oceanography **76**(4): 399-442.

Durski, S. M., S. M. Glenn and D. B. Haidvogel (2004). "Vertical mixing schemes in the coastal ocean: Comparison of the level 2.5 Mellor-Yamada scheme with an enhanced version of the K profile parameterization." Journal of Geophysical Research: Oceans **109**(C1): C01015.

Ganf, G. G. (1974). "Diurnal Mixing and the Vertical Distribution of Phytoplankton in a Shallow Equatorial Lake (Lake George, Uganda)." Journal of Ecology **62**(2): 611-629.

Henderson-Sellers, B. (1985). "New formulation of eddy diffusion thermocline models." Applied Mathematical Modelling **9**(6): 441-446.

Henderson-Sellers, B. (1986). "Calculating the surface energy balance for lake and reservoir modeling: A review." Reviews of Geophysics **24**(3): 625-649.

Huisman, J., P. v. Oostveen and F. J. Weissing (1999). "Critical Depth and Critical Turbulence: Two Different Mechanisms for the Development of Phytoplankton Blooms." Limnology and Oceanography **44**(7): 1781-1787.

Imboden, D. M., U. Lemmin, T. Joller and M. Schurter (1983). "Mixing processes in lakes: mechanisms and ecological relevance." Schweizerische Zeitschrift für Hydrologie **45**(1): 11-44.

Imerito, A. (2007). Dynamic reservoir simulation model. DYRESM v 4.0 science manual, University of Western Australia.

Ivey, G. N. and J. Imberger (1991). "On the Nature of Turbulence in a Stratified Fluid. Part I: The Energetics of Mixing." Journal of Physical Oceanography **21**(5): 650-658.

Jassby, A. and T. Powell (1975). "Vertical Patterns of Eddy Diffusion During Stratification in Castle Lake, California." Limnology and Oceanography **20**(4): 530-543.

Lewis, W. M. (1996). Tropical lakes: how latitude makes a difference. Perspectives in tropical Limnology. F. B. Schiemer, K T. Amsterdam, The Netherlands, SPB Academic Publishing 43-64.

Lewis, W. M., Jr. (1982). "Vertical Eddy Diffusivities in a Large Tropical Lake." Limnology and Oceanography **27**(1): 161-163.

Lo, E. Y. M. (2008). Water quality monitoring, modeling and management for Kranji catchment/reservoir system. Singapore, Public Utilites Board.

MacIntyre, S. (1993). "Vertical Mixing in a Shallow, Eutrophic Lake: Possible Consequences for the Light Climate of Phytoplankton." Limnology and Oceanography **38**(4): 798-817.

MacIntyre, S., K. M. Flynn, R. Jellison and J. R. Romero (1999). "Boundary mixing and nutrient fluxes in Mono Lake, California." Limnology and Oceanography **44**(3): 512-529.

MacIntyre, S. and J. M. Melack (1982). "Meromixis in an Equatorial African Soda Lake." Limnology and Oceanography **27**(4): 595-609.

Monismith, S. G., J. Imberger and M. L. Morison (1990). "Convective motions in the sidearm of a small reservoir." Limnol. Oceanogr **35**(8): 1676-1702.

Moon, P. (1940). "Proposed standard solar-radiation curves for engineering use." Journal of the Franklin Institute **230**(5): 583-617.

Osborn, T. R. (1980). "Estimates of the Local Rate of Vertical Diffusion from Dissipation Measurements." Journal of Physical Oceanography **10**(1): 83-89.

Osborn, T. R. and C. S. Cox (1972). "Oceanic fine structure." Geophysical Fluid Dynamics **3**(1): 321-345.

Pope, S. B. (2000). Turbulent Flows, Cambridge University Press.

Shih, L. H., J. R. Koseff, G. N. Ivey and J. H. Ferziger (2005). "Parameterization of turbulent fluxes and scales using homogeneous sheared stably stratified turbulence simulations." Journal of Fluid Mechanics **525**: 193-214.

Sverdrup, H. U., M. W. Johnson and R. H. Fleming (1942). The Oceans Their Physics, Chemistry, and General Biology. New York, Prentice-Hall, Inc.

Tsubo, M. and S. Walker (2005). "Relationships between photosynthetically active radiation and clearness index at Bloemfontein, South Africa." Theoretical and Applied Climatology **80**(1): 17-25.

Wong, K. T. M., J. H. W. Lee and I. J. Hodgkiss (2007). "A simple model for forecast of coastal algal blooms." Estuarine, Coastal and Shelf Science **74**(1-2): 175-196.

Xing, Z., D. A. Fong, E. Y.-M. Lo and S. G. Monismith (2014). "Thermal structure and variability of a shallow tropical reservoir." Limnol. Oceanogr **59**(1): 115-128.

Xing, Z., D. A. Fong, K. M. Tan, E. Y.-M. Lo and S. G. Monismith (2012). "Water and heat budgets of a shallow tropical reservoir." Water Resources Research **48**(6): W06532.

Yeates, P. S. and J. Imberger (2003). "Pseudo two-dimensional simulations of internal and boundary fluxes in stratified lakes and reservoirs." International Journal of River Basin Management **1**(4): 297 - 319.

Table Caption

Table 1: Three distinct regimes of turbulence behaviour defined by Shih et al. (2005)

Table 2: the depth-median K_z values in the surface mixed layer, thermocline, and the lower water column during the two SCAMP days of Sept 29/30 and Oct 05/06 2011

Figure Caption

Figure 1: Kranji Reservoir with mooring stations

Figure 2: A: vertical temperature profiles at M4, M5 and M6 during 5:00-9:00 on day 110 of 2007; B: K_z for 7:00-9:00 on day 110 of 2007 and C: the short-wave radiation during day 108-112 of 2007; the intervals between the dash lines highlight the isolation during the 11:00-15:00 time period.

Figure 3: Calculated heat flux (W/m^2) between the water column and the sediment at M5.

Figure 4: Vertical temperature at M4, M5 and M6 in Kranji Reservoir during 11:00-15:00 and K_z values for the 2hr period from 13:00-15:00 on day 110 of 2007. The lines with circles denote the temperature profiles averaged over 11:00-13:00 while the lines with squares denote the temperature profiles averaged over 13:00-15:00. Error bars in K_z show the uncertainties induced by the instrument errors.

Figure 5: Median vertical eddy diffusivities (K_z) as a function of depth at M4, M5 and M6 during 11:00 to 15:00 over 43 solar regime days. The bars cover the ranges from the 1st quartile to the 3rd quartile of K_z values.

Figure 6: Median vertical eddy diffusivities (K_z) profiles during different forcing regimes. Note that 2 profiles over 11:00 to 15:00 are used for each day.

Figure 7: Hydro-meteorological conditions (short-wave radiation, wind speed, inflow and rainfall) during two 24hr SCAMP measurements and inflow and rainfall amount spanning from Sept 27-Oct 9 in 2011.

Figure 8: Water temperature, surface-bottom temperature difference and velocity along the channel during the two 24hr SCAMP measurements. Black lines indicate temperature contours with a contour level of 0.2 ^oC during Sept 29/30 and of 0.5 ^oC during Oct 5/6.

Figure 9: Vertical eddy diffusivities derived from SCAMP measured χ_T, Richardson number and turbulent intensity parameter in log scales during 24hr SCAMP measurements of Sept 29/30 and Oct 05/06 2011. Black lines indicate temperature contours with a contour level of 0.2 ^oC during Sept 29/30 and of 0.5 ^oC during Oct 5/6.

Figure 10: A: Depth profile of the temperature measured by SCAMP during 11:00-15:00 of Sept 29 2011. The solid line with circles denotes the temperature profile averaged over 11:00-13:00 and the dotted line with squares denotes the temperature profile average over 13:00-15:00. B: Depth profile of K_z derived from χ_T measured by SCAMP during the same period. The bars indicate show the upper and the lower quartile values, with the vertical line indicating the median value. The dashed lines indicate the minimum/maximum values. Two lines superimposed on the boxplot denote the K_z profiles calculated from the heat flux method with the solid line with circles for 11:00-13:00 and the dotted line with squares for 13:00-15:00.

Regime	$\varepsilon / \nu N^2$ **range**	**Behavior of turbulence**
Diffusive	$\varepsilon / \nu N^2 < 7$	turbulence decaying
Intermediate	$7 < \varepsilon / \nu N^2 < 100$	turbulence in equilibrium
Energetic	$\varepsilon / \nu N^2 > 100$	energetic turbulence, turbulence growing

Table 1

The median of K_z (m^2/s) over the depth of	during the heating period of Sept 29 (11:00-19:00)	during the non-heating of Sept 29/30 (19:00-7:00)	during the heating period of Oct 5 (12:00-19:00)	during the non-heating period of Oct 5/6 (19:00-7:00)
Surface mixed layer	2.3×10^{-4}	2.0×10^{-4}	2.1×10^{-5}	2.3×10^{-6}
Thermocline	2.8×10^{-5}		7.4×10^{-7}	4.3×10^{-7}
Lower water column	2.8×10^{-4}	3.1×10^{-4}	1.6×10^{-5}	8.5×10^{-5}
The whole water column	1.8×10^{-4}	2.9×10^{-4}	3.6×10^{-6}	3.5×10^{-6}

Table 2

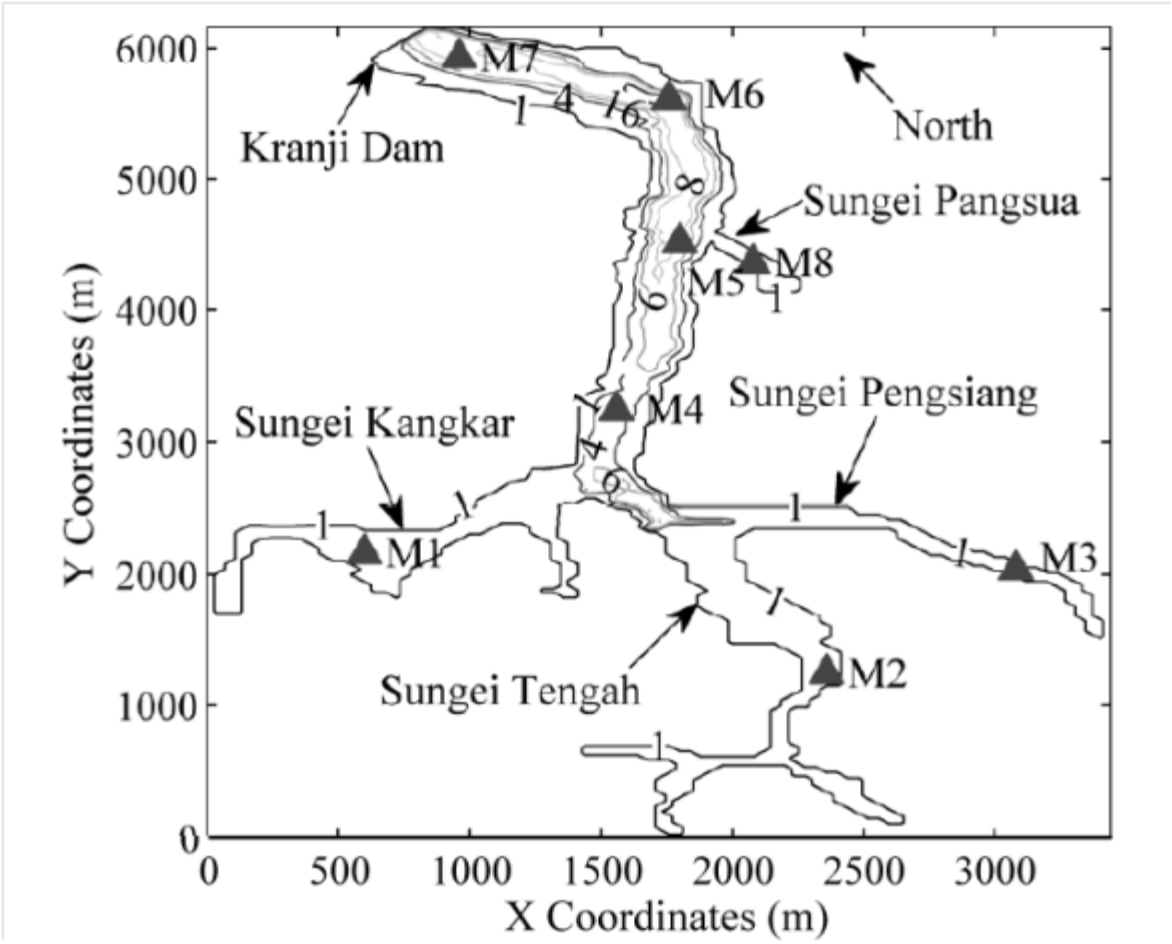
M7
M6
M8
M5
M4
M1
M3
M2
Kranji Dam
North
Sungei Pangsua
Sungei Kangkar
Sungei Pengsiang
Sungei Tengah
Y Coordinates (m)
X Coordinates (m)
0
1000
2000
3000
4000
5000
6000
0
500
1000
1500
2000
2500
3000

Figure 1

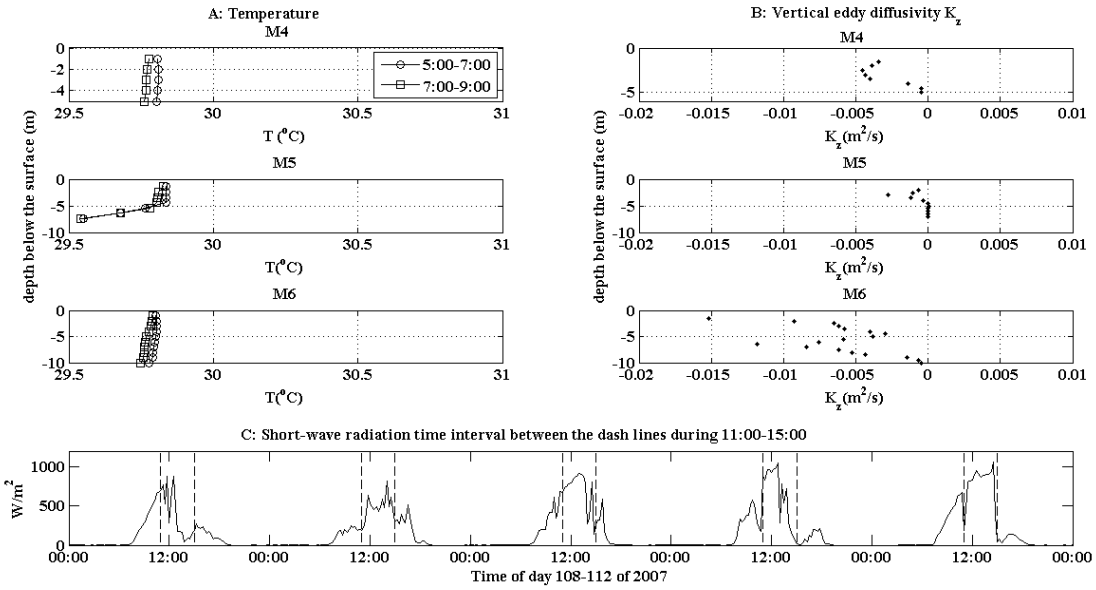
A: Temperature
M4
5:00-7:00
7:00-9:00
T (°C)
M5
T(°C)
M6
T(°C)
depth below the surface (m)
B: Vertical eddy diffusivity K_z
M4
K_z(m^2/s)
M5
K_z(m^2/s)
M6
K_z(m^2/s)
depth below the surface (m)
C: Short-wave radiation time interval between the dash lines during 11:00-15:00
W/m^2
Time of day 108-112 of 2007

Figure 2

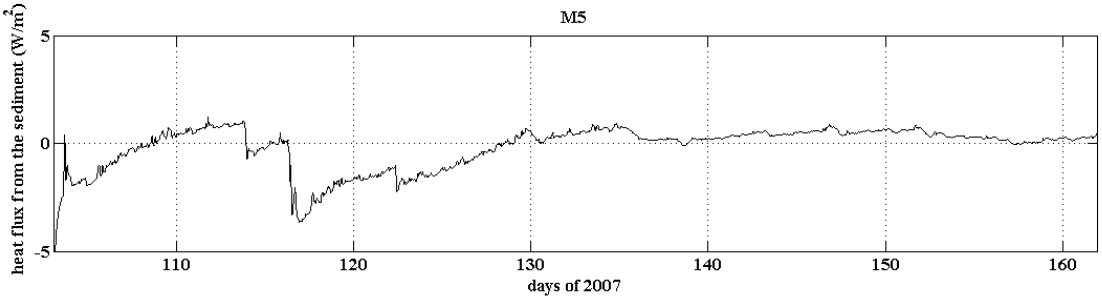
M5
heat flux from the sediment (W/m²)
5
0
-5
110
120
130
140
150
160
days of 2007

Figure 3

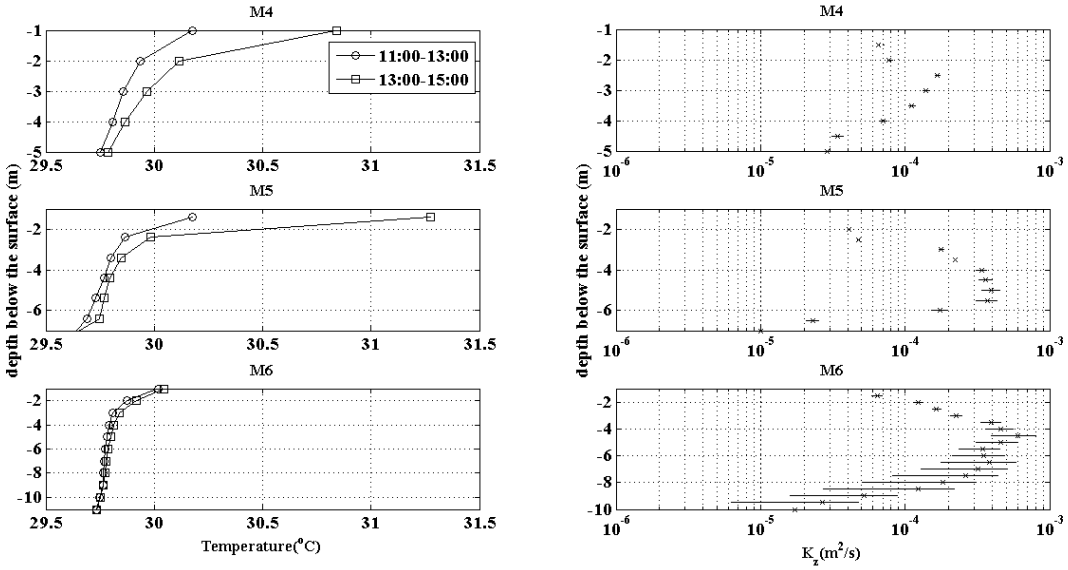
M4
M5
M6
11:00-13:00
13:00-15:00
depth below the surface (m)
Temperature(°C)
K_z(m²/s)

Figure 4

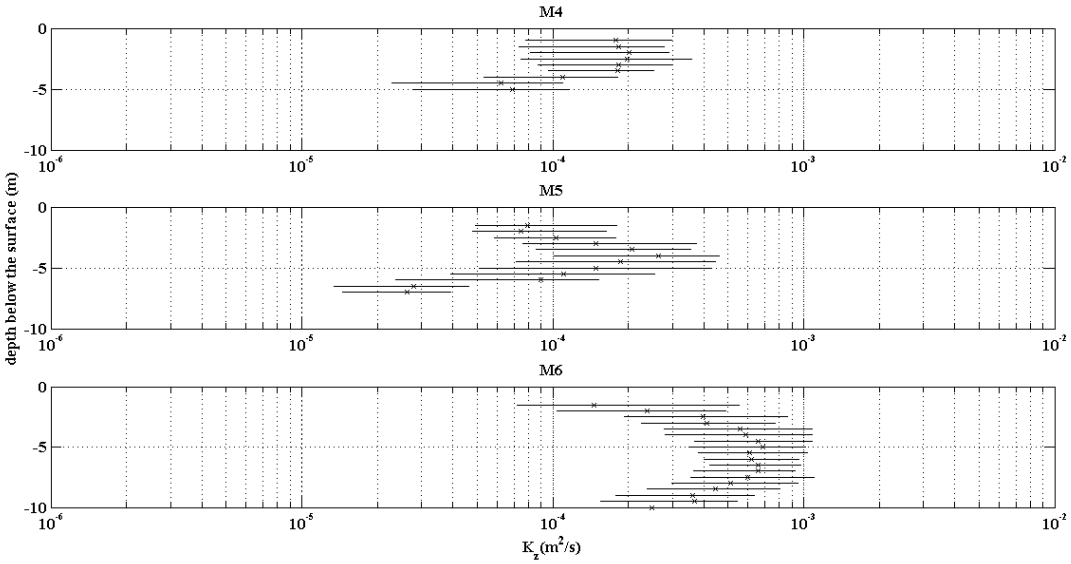
M4
M5
M6
depth below the surface (m)
0
-5
-10
10^{-6}
10^{-5}
10^{-4}
10^{-3}
10^{-2}
$K_z (m^2/s)$

Figure 5

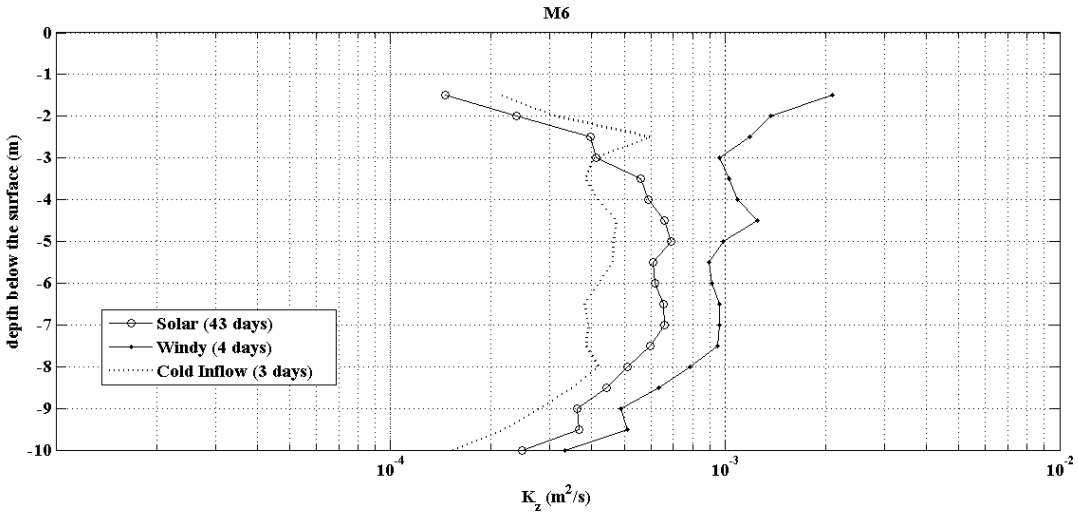
M6
depth below the surface (m)
0
-1
-2
-3
-4
-5
-6
-7
-8
-9
-10
Solar (43 days)
Windy (4 days)
Cold Inflow (3 days)
10^-4
10^-3
10^-2
K_z (m^2/s)

Figure 6

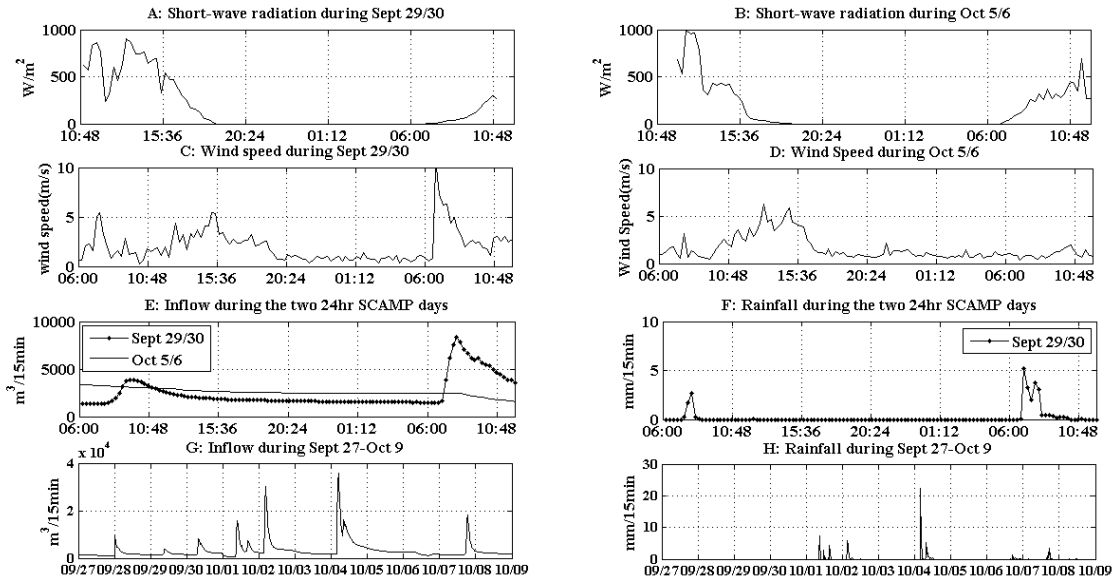
A: Short-wave radiation during Sept 29/30
W/m2
1000
500
0
10:48
15:36
20:24
01:12
06:00
10:48
B: Short-wave radiation during Oct 5/6
C: Wind speed during Sept 29/30
wind speed(m/s)
10
5
0
06:00
10:48
15:36
20:24
01:12
06:00
10:48
D: Wind Speed during Oct 5/6
Wind Speed(m/s)
E: Inflow during the two 24hr SCAMP days
m3/15min
10000
5000
Sept 29/30
Oct 5/6
F: Rainfall during the two 24hr SCAMP days
mm/15min
Sept 29/30
G: Inflow during Sept 27-Oct 9
x 10^4
4
2
09/27 09/28 09/29 09/30 10/01 10/02 10/03 10/04 10/05 10/06 10/07 10/08 10/09
H: Rainfall during Sept 27-Oct 9
30
20
10

Figure 7

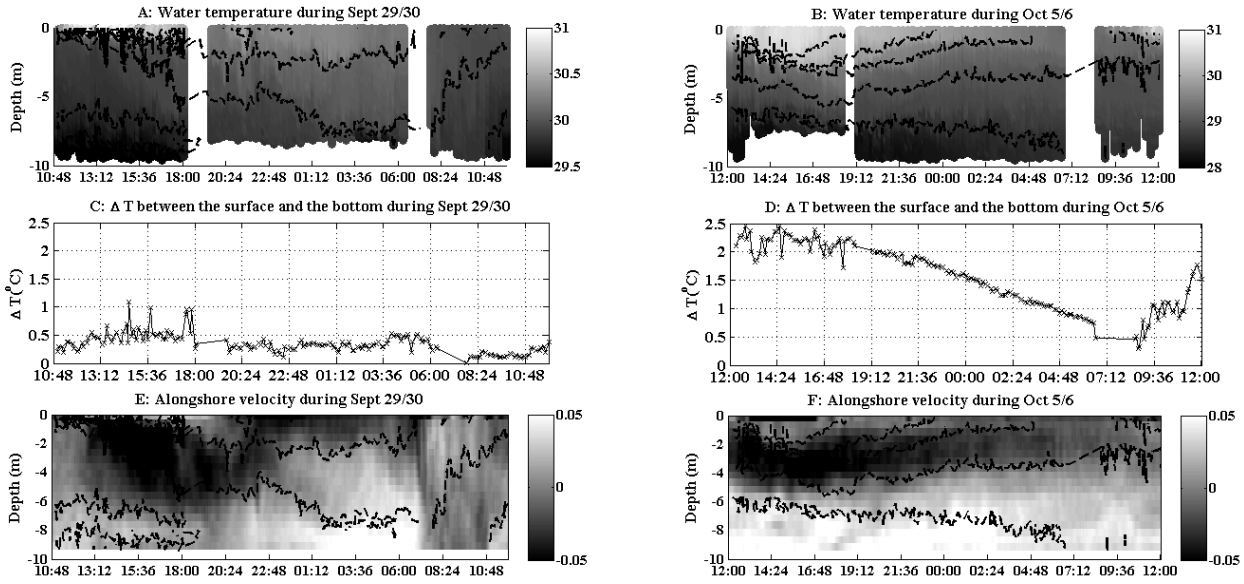
A: Water temperature during Sept 29/30
Depth (m)
0
-5
-10
31
30.5
30
29.5
10:48 13:12 15:36 18:00 20:24 22:48 01:12 03:36 06:00 08:24 10:48
B: Water temperature during Oct 5/6
Depth (m)
0
-5
-10
31
30
29
28
12:00 14:24 16:48 19:12 21:36 00:00 02:24 04:48 07:12 09:36 12:00
C: Δ T between the surface and the bottom during Sept 29/30
Δ T(°C)
2.5
2
1.5
1
0.5
0
10:48 13:12 15:36 18:00 20:24 22:48 01:12 03:36 06:00 08:24 10:48
D: Δ T between the surface and the bottom during Oct 5/6
Δ T(°C)
2.5
2
1.5
1
0.5
0
12:00 14:24 16:48 19:12 21:36 00:00 02:24 04:48 07:12 09:36 12:00
E: Alongshore velocity during Sept 29/30
Depth (m)
0
-2
-4
-6
-8
-10
0.05
0
-0.05
10:48 13:12 15:36 18:00 20:24 22:48 01:12 03:36 06:00 08:24 10:48
F: Alongshore velocity during Oct 5/6
Depth (m)
0
-2
-4
-6
-8
-10
0.05
0
-0.05
12:00 14:24 16:48 19:12 21:36 00:00 02:24 04:48 07:12 09:36 12:00

Figure 8

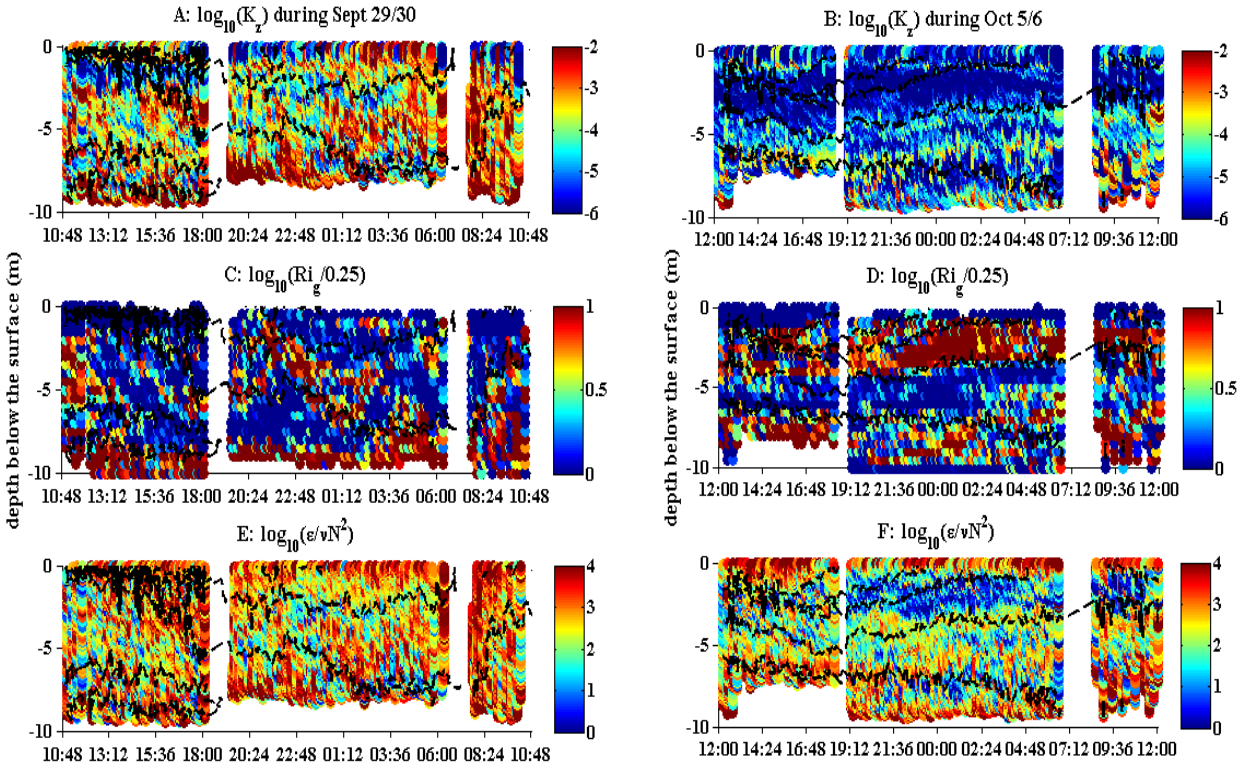
A: log10(Kz) during Sept 29/30
B: log10(Kz) during Oct 5/6
C: log10(Rig/0.25)
D: log10(Rig/0.25)
E: log10(ε/νN2)
F: log10(ε/νN2)
depth below the surface (m)
depth below the surface (m)
0
-5
-10
-2
-3
-4
-5
-6
1
0.5
0
4
3
2
1
0
10:48 13:12 15:36 18:00 20:24 22:48 01:12 03:36 06:00 08:24 10:48
12:00 14:24 16:48 19:12 21:36 00:00 02:24 04:48 07:12 09:36 12:00

Figure 9

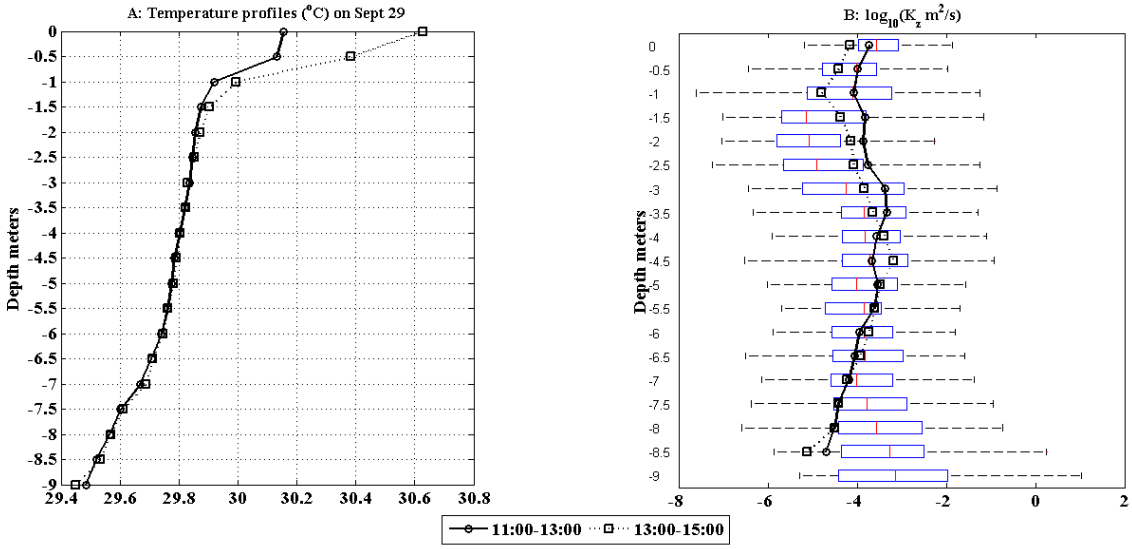
A: Temperature profiles (°C) on Sept 29
Depth meters
0
-0.5
-1
-1.5
-2
-2.5
-3
-3.5
-4
-4.5
-5
-5.5
-6
-6.5
-7
-7.5
-8
-8.5
-9
29.4
29.6
29.8
30
30.2
30.4
30.6
30.8
B: log10(Kz m2/s)
-8
-6
-4
-2
0
2
11:00-13:00
13:00-15:00

Figure 10